1720 *Inorg. Chem.* **2010**, *49*, 1720–1727
DOI: 10.1021/ic9019316

Inorganic Chemistry
Article

Organometallic Trinuclear Niobium Cluster Complex in Aqueous Solution: Synthesis and Characterization of Niobium Complexes Containing $Nb_3(\mu\text{-}\eta^2{:}\eta^2(\perp)\text{-}NCCH_3)(\mu_2\text{-}O)_3^{6+}$ Cluster Core

Hans Arni Nybo Joensen,[†] Gro Kallehave Hansson,[†] Svetlana G. Kozlova,[‡] Artem L. Gushchin,[†] Inger Søtofte,*[,†] and Bee-Lean Ooi[†,§]

[†]*Department of Chemistry, Technical University of Denmark, Building 207, Kemitorvet, 2800 Lyngby, Denmark, and* [‡]*Nikolaev Institute of Inorganic Chemistry, Siberian Branch of the Russian Academy of Sciences, Lavrentiev Avenue 3, Novosibirsk 630090, Russia.* [§]*The main author, deceased November 2009*

Received October 1, 2009

The synthesis and characterization of an organometallic trinuclear oxo-bridged niobium cluster complex with perpendicularly coordinated $\mu_3\text{-}\eta^2{:}\eta^2(\perp)$-acetonitrile ligand in aqueous solution is reported. Reaction of $NbCl_5$ in acetonitrile with aluminum under argon followed by reaction with aqueous hydrochloric acid affords, after suitable workup, the isolation of the organometallic $[Nb_3(\mu\text{-}\eta^2{:}\eta^2\text{-}NCCH_3)O_3(H_2O)_9]^{6+}$ aqua ion by cation-exchange chromatography. The purple niobium aqua ion in 2 M HCl shows a small peak at 365 nm ($\varepsilon \sim 511\ M^{-1}\ cm^{-1}$ per Nb) and a broad peak at 565 nm ($\varepsilon \sim 335\ M^{-1}\ cm^{-1}$) in the UV−visible region. It is electron paramagnetic resonance (EPR)-active ($g = 1.98$), but no hyperfine interaction with the ^{93}Nb nuclear spin ($I = 9/2$) was observed. The cyclic voltammogram of $[Nb_3(\mu\text{-}\eta^2{:}\eta^2\text{-}NCCH_3)O_3(H_2O)_9]^{6+}$ in 4 M HCl on edge-plane pyrolytic graphite electrode at 50 mV s^{-1} in the potential range −1.2 V to +1.1 V (vs SCE) exhibits three anodic peaks at −0.12, +0.53, and +0.85 V and a large cathodic peak at −0.91 V with a slight shoulder at about −0.8 V. The purple aqua ion reacted with potassium thiocyanate to give the green thiocyanate derivative, which was crystallized as $((CH_3)_3NH)_3[Nb_3(\mu\text{-}\eta^2{:}\eta^2\text{-}NCCH_3)O_3(NCS)_9]\cdot 2.5H_2O$ (**1**) and subjected to X-ray structure analysis. Density-functional theory (DFT) calculations fully supported the structure of the cluster.

Introduction

This work is very interesting to us for three reasons: first, organometallic cluster aqua ions are rare, second the perpendicularly coordinated $\mu_3\text{-}\eta^2{:}\eta^2(\perp)$-acetonitrile ligand is unusual, and finally only few aqua ions of niobium are known.

Aqueous organometallic chemistry is attracting growing attention for applications in catalysis because water is an environmentally friendly and benign medium. Since the report of the earliest examples of organometallic aqua ions, $[(C_6H_6)Ru(H_2O)_3]^{2+}$ and $[(C_6H_6)Os(H_2O)_3]^{2+}$,[1] there has been a steady increase in the number of organometallic aqua ions.[2] They contain mainly a single metal center except for a few examples with dimetallic and trimetallic centers.[3,4] The existence of stable organometallic aqua ions will lend further support to the increasing potential and scope of aqueous organometallic chemistry since the labile aqua ligands can serve as open sites for substrate binding and activation.

The title compound, $[Nb_3(\mu\text{-}\eta^2{:}\eta^2\text{-}NCCH_3)O_3(H_2O)_9]^{6+}$ aqua ion, was formed serendipitiously in a reaction whereby acetonitrile was used as solvent in the first step. The acetonitrile ligand is coordinated perpendicularly as $\mu_3\text{-}\eta^2{:}\eta^2(\perp)$. Although an example of this unusual coordination geometry of a nitrile has recently been reported in $(Cp^*Ru)_3(\mu_3\text{-}\eta^2{:}\eta^2\text{-}(\perp)\text{-}RCN)(\mu_3\text{-}H)(\mu\text{-}H)_2$ (R = Ph, ^{t}Bu),[5] what makes it unique is that our complex is stable in aqueous solution. Furthermore, the triniobium cluster aqua ion is the first and only example of an organometallic species whereby there are several peripheral ligands around each metal, all completely water ligands. This is in contrast to for example the μ_3-alkylidyne capped molybdenum acetate complex, $[Mo_3(CCH_3)_2(CH_3COO)_6(H_2O)_3]^{2+}$, where there is only one terminal water ligand per metal center.[3] Nevertheless the relatively labile water ligands in

*To whom correspondence should be addressed. E-mail: is@elten.dk.

(1) Hung, Y.; Kung, W. J.; Taube, H. *Inorg. Chem.* **1981**, *20*, 457–463.
(2) Koelle, U. *Coord. Chem. Rev.* **1994**, *135/136*, 623–650.
(3) (a) Bino, A.; Cotton, F. A.; Dori, Z. *J. Am. Chem. Soc.* **1981**, *103*, 243–244. (b) Ardon, M.; Bino, A.; Cotton, F. A.; Dori, Z.; Kaftory, M.; Kolthammer, B. W. S.; Kapon, M.; Reisner, G. *Inorg. Chem.* **1981**, *20*, 4083–4090.
(4) (a) Dinoi, C.; Prikhodchenko, P.; Demirhan, F.; Gun, J.; Lev, O.; Daran, J.-C.; Poli, R. *J. Organomet. Chem.* **2007**, *692*, 2599–2605. (b) Dinoi, C.; Sözen, P.; Taban, G.; Demir, D.; Demirhan, F.; Prikhodchenko, P.; Gun, J.; Lev, O.; Daran, J.-C.; Poli, R. *Eur. J. Inorg. Chem.* **2007**, 4306–4316. (c) Demirhan, F.; Cagatay, B.; Demir, D.; Baya, M.; Daran, J.-C.; Poli, R. *Eur. J. Inorg. Chem.* **2006**, 757–764.
(5) Takao, T.; Kawashima, T.; Matsubara, K.; Suzuki, H. *Organometallics* **2005**, *24*, 3371–3374.

 Published on Web 02/08/2010

the trimolybdenum cluster are believed to play an important role in the coupling reaction of the alkylidyne ligands upon reaction of $[Mo_3(CCH_3)_2(CH_3COO)_6(H_2O)_3]^{2+}$ with aqueous HBr resulting in a μ_3-$\eta^2(\perp)$-alkyne ligand in the product, $[Mo_3Br_7(CH_3COO)(H_2O)_2(H_3C{\equiv}CCH_3)]$.[6] Recently there has been a concerted effort toward the development of the chemistry of high-valent organometallic compounds in water which resulted in several oxo-supported high-valent organometallic complexes.[4] However, the peripheral ligands in all these complexes are cyclopentadienyls.

The aqueous solution chemistry of niobium remains largely unexplored. To date only four niobium aqua ions have been reported,[7−10] and for three of them the incomplete cuboidal oxo-bridged triniobium, $Nb_3(\mu_3\text{-}X)(\mu_2\text{-}O)_3$, framework prevails. There had been uncertainty on the identity of the μ_3-ligand for the first isolated aqua ion of niobium, purportedly the green $[Nb_3(\mu_3\text{-}O)(\mu_2\text{-}O)_3(H_2O)_9]^{3+}$ ion, which upon reaction with thiocyanate crystallized as $(NH_4)_3(Me_4N)_3[Nb_3(\mu_3\text{-}S)(\mu_2\text{-}O)_3(NCS)_9]\cdot MeOH$ whereby a sulphide ends up in the capping μ_3-position.[7] Later evidence by a niobium K edge extended x-ray absorption fine structure (EXAFS) study on samples obtained following evaporation to dryness of HCl solutions of the green aqua ion and dissolution in CF_3SO_3H favors the formulation of $[Nb_3(\mu_3\text{-}Cl)(\mu_2\text{-}O)_3(H_2O)_9]^{4+}$.[11] These observations suggest high lability of the μ_3-ligand of the $Nb_3(\mu_3\text{-}X)(\mu_2\text{-}O)_3$ core, and the isolation of the $[Nb_3(\mu\text{-}\eta^2{:}\eta^2\text{-}NCCH_3)O_3(H_2O)_9]^{6+}$ aqua ion further corroborates this suggestion.

We report herein the synthesis and characterization of a novel organometallic triniobium aqua ion and X-ray structure analysis of the thiocyanate derivative complex.

Experimental Section

Starting Materials. All commercially available chemicals were used as received. The synthesis and manipulations of the niobium products were carried out under an oxygen-free atmosphere. Standard oxygen-free techniques involving use of argon, rubber septa, Teflon tubing and needles, syringes, as well as glovebag techniques, were routinely employed.

Preparation of $[Nb_3(\mu\text{-}\eta^2{:}\eta^2\text{-}NCCH_3)O_3(H_2O)_9]^{6+}$ Aqua Ion. Niobium pentachloride (2.5 g) was dissolved in 25 mL of acetonitrile, and reduction was carried out using aluminum powder (0.5 g) under stirring. The solution turned from yellow to brown after 2 to 3 days. The resultant dark brown solution was filtered to remove the excess aluminum, and the reduced mixture added to 4 M HCl (50 mL) to give a dark purplish brown solution. After 5-fold dilution with water, the solution was adsorbed on a Dowex 50W-X2 cation-exchange column (2.2 cm × 45 cm). A dark reddish purple band bound and a light brown unbound species spread throughout the column and was removed by washing with 0.8 M HCl. Upon washing with 3−4 M HCl the purple aqua ion was eluted. A dark reddish purple band remained on the column. Yields at this stage were typically about 50−60% based on niobium.

Further purification of the purple aqua ion on a Dowex 50W-X2 column (2.2 cm × 35 cm) was carried out by dilution to $[H^+]$ = 0.8 M HCl. A dark reddish purple band on the top of the column and a light purple more loosely bound band were observed. Upon washing with 1 M HCl, a light purple fraction was eluted. Further washing with 2 M HCl gave yet another but more concentrated purple fraction followed by a small amount of grayish brown species (not investigated further). A dark reddish purple band remained on top of the column, and upon washing with 3 or 4 M HCl, yet another purple fraction was eluted. This continued when the column was left to stand in 3 or 4 M HCl, giving several fractions of purple solutions until the dark band on the top of the column became progressively lighter in color. All the purple fractions have similar UV−visible spectra. When cation-exchange chromatography was carried out with non-coordinating HPTS (paratoluenesulphonic acid), a purple fraction was eluted in 2 M HPTS while a dark reddish purple band remained bound. No further colored fractions were obtained even upon washing with 4 M HPTS. However, when 3−4 M HCl was used, the purple fractions began eluting from the dark reddish purple band in the manner described above. Solutions of the aqua ion used for investigations were the purple fractions obtained upon elution with 2 M HCl, which were further concentrated on a Dowex 50W-X2 column followed by elution with 4 M HCl. Solutions obtained in this manner were used for all investigations.

UV−visible Spectrum and Dependence on $[H^+]$ and $[Cl^-]$. All UV−visible spectra were recorded on a Hewlett-Packard 8453 diode-array spectrophotometer. In 2 M HCl, a small peak at 365 nm ($\varepsilon \sim 511\ M^{-1}\ cm^{-1}$) and a broad peak at 565 nm ($\varepsilon \sim 335\ M^{-1}\ cm^{-1}$) were observed. ε values (per Nb) are based on Nb analysis by either ICP-AES or ICP-MS. The peak at 365 nm reduces to a shoulder in 1 M HCl but becomes very prominent and increases in intensity in 4 M HCl. When a purple solution of the aqua ion in 1 or 2 M HCl was attached to a vacuum-line, a clear color change was observed from purple to grayish purple and finally giving a dark green solid.

Since the UV−visible spectrum of the purple aqua ion is very sensitive to the concentration of HCl, the independent influence of $[H^+]$ and $[Cl^-]$ on the UV−visible spectrum were investigated by monitoring the spectrum while varying the concentration of one and maintaining the concentration of the other (See Supporting Information). The concentration of Nb was kept constant at about 1 mM. A 6 M solution of NaCl was used to adjust $[Cl^-]$ while 5 M HPTS was used to vary $[H^+]$.

Preparation of $((CH_3)_3NH)_3[Nb_3(\mu\text{-}\eta^2{:}\eta^2\text{-}NCCH_3)O_3(NCS)_9]\cdot 2.5H_2O$ (1). Crystals of **1** were obtained by adding solid KNCS (75 mg) to a solution of the purple aqua ion (2.5 mM per Nb, 1.5 mL) in 4 M HCl. The color of the solution turned immediately to dark green. After standing for an hour under argon at room temperature, an aqueous solution of $(CH_3)_3NHCl$ (650 mg in 1 mL water) was then carefully layered on the top. After 2−3 days at 4 °C, dark green brown crystals of **1**, suitable for X-ray crystallography were deposited. Calcd for $C_{20}H_{38}N_{13}Nb_3O_{5.50}S_9$: C 21.53; H 3.43; N 16.32. Found: C 23.84, H 4.00, N 16.56. Note: The higher experimental values were not very satisfactory and were due to problems faced in and upon washing the crystals. The ready solubility of the crystals in various solvents including water, methanol, and ethanol hampered thorough washing. Hence the crystals were washed only twice with cold water (which to complicate matters further gives off the purple color of the aqua ion indicating the high lability of the thiocyanate ligand) and then dried under argon over concentrated sulphuric acid. Furthermore, the crystals are air-sensitive, but the elemental analysis was carried out in air.

X-ray Crystallography. Under a protective layer of paraffin oil, a dark green brown crystal of **1** (0.41 × 0.08 × 0.05 mm) was selected and mounted on a glass fiber. The crystal was then cooled to 120 K using a Cryostream nitrogen gas cooler system,

(6) Bino, A.; Ardon, M.; Shirman, E. *Science* **2005**, *308*, 234–235.
(7) Cotton, F. A.; Diebold, M. P.; Llusar, R.; Roth, W. J. *J. Chem. Soc., Chem. Commun.* **1986**, 1276.
(8) Sokolov, M. N.; Hernandez-Molina, R.; Elsegood, M. R. J.; Heath, S. L.; Clegg, W.; Sykes, A. G. *J. Chem. Soc., Dalton Trans.* **1997**, 2059.
(9) Ooi, B. L.; Søtofte, I.; Bendtsen, M. F.; Munch, A.; Nielsen, L. C.; Henriksen, J. *Inorg. Chem.* **2005**, *44*, 480–482.
(10) Ooi, B. L.; Søtofte, I.; Sokolov, M. N.; Kozlova, S. G.; Rasmussen, S. B.; Nielsen, L. C.; Henriksen, J. *Inorg. Chem.* **2006**, *45*, 5008–5017.
(11) Richens, T. R.; Shannon, I. J. *J. Chem. Soc., Dalton Trans.* **1998**, 2611.

Table 1. Crystallographic Data for $((CH_3)_3NH)_3[Nb_3(\mu\text{-}\eta^2\text{:}\eta^2\text{-}NCCH_3)O_3(NCS)_9]\cdot 2.5H_2O$ (**1**)

formula	$C_{20}H_{38}N_{13}Nb_3O_{5.50}S_9$
formula weight	1115.90
crystal system, color	triclinic, dark green brown
crystal dimension (mm)	$0.41 \times 0.08 \times 0.05$
space group	$P\bar{1}$
a (Å)	13.269(2)
b (Å)	13.943(2)
c (Å)	17.524(2)
α (deg)	74.754(3)
β (deg)	86.141(3)
γ (deg)	62.668(3)
V (Å^3)	2773.4(7)
Z	2
D_c (g cm^{-3})	1.336
μ (Mo−K$_\alpha$, λ = 0.71070 Å) (mm^{-1})	0.985
no. of measured reflections	19836
no. of unique reflections	12327
no. of reflections with $I > 2\sigma(I)$	7125
R(int)	0.05(10)
transmission factors	1.0000−0.4298
no. of refined parameters	540
R_1 (observed data)[a]	0.0933
wR_2 (all data)[b]	0.3041
goodness-of-fit	1.030
max, min $\Delta\rho$ (e Å^{-3})	1.727, −1.017

[a] $R_1 = \sum||F_o| - |F_c||/\sum|F_o|$. [b] $wR_2 = [\sum w(F_o^2 - F_c^2)^2/\sum wF_o^4]^{1/2}$.

and data were collected on a Siemens SMART platform diffractometer with a CCD area sensitive detector. The crystallographic data and details of diffraction experiments are given in Table 1. The structure was solved by direct methods and refined by full-matrix least-squares against F^2 of all data. Eight of the sulfur atoms are disordered and split between two positions with population factors for S(1A) and S(1A)′ of 0.668(9)and 0.332(9), for S(2A) and S(2A)′ 0.94(3) and 0.06(3), for S(3A) and S(3A)′ 0.87(3) and 0.13(3), for S(1B) and S(1B)′ 0.766(9) and 0.234(9), for S(2B) and S(2B)′ 0.921(12) and 0.079(12), for S(3B) and S(3B)′ 0.837(10) and 0.163(10), for S(2C) and S(2C)′ 0.84(7) and 0.16(7), for S(3C) and S(3C)′ 0.65(3) and 0.35(3), respectively. In the disordered NCS groups the S atoms were refined with equal C−S bonds with an effective standard deviation of 0.02. The temperature factors of S(3B) and S(3B)′ are rather large and may indicate that the atoms are disordered. The population factors for the water molecules were for O(10), O(20) and O(10)′, O(20)′ 0.632(12) and 0.368(12) and for O(30) and O(30)′ 0.338(12) and 0.162(12), respectively.

In the trimethylammonium ions the positions of some of the atoms may split up, but the positions reported here, with population factors of 1.0 for the $(CH_3)_3N(2)H$ and the $(CH_3)_3N(3)H$ ions and 0.5 for the $(CH_3)_3N(4)H$ and the $(CH_3)_3N(5)H$ ions, were found to give a reasonable model. The modifications of the positions and the population factors of the cations do not change the structure of the cluster anion.

The non-hydrogen atoms were refined anisotropically. The positions of the hydrogen atoms of the trimethylammonium ions were at calculated positions using a riding model with C−H = 0.98 Å and N−H = 0.93 Å. For all hydrogen atoms the thermal parameters were fixed [U_{iso}(H) = 1.2U_{iso}(C,N)]. The hydrogen atoms of the water molecules were neither found nor calculated and therefore not included in the refinement. Programs used for data collection, data reduction and absorption were SMART v. 5.05, SAINT v. 6.02, and SADABS v. 2.03.[12,13] The program SHELXTL v. 6.12[14] was used to solve the structure and for molecular graphics.

Charge Determination. The well characterized molybdenum aqua ions, $[Mo_3S_4(H_2O)_9]^{4+}$, $[Mo_4S_4(H_2O)_{12}]^{5+}$, and $[Mo_7S_8(H_2O)_{18}]^{8+}$ were used as references. The purple niobium aqua ion (in excess of $[Mo_4S_4(H_2O)_{12}]^{5+}$ since it reduces the Mo aqua ion to $[Mo_4S_4(H_2O)_{12}]^{4+}$) was mixed with the reference complexes and loaded onto a Dowex 50W-X2 column after dilution to 0.75 M HCl. The column was developed by washing with 0.75, 0.8, 1, 1.5, 2, 2.5, and finally 4 M HCl. The leafy green $[Mo_3S_4(H_2O)_9]^{4+}$ eluted first, followed by a faint pinkish purple band of probably a chloro species of the purple niobium aqua ion, and then very closely by the orange $[Mo_4S_4(H_2O)_{12}]^{4+}$. The deep green $[Mo_4S_4(H_2O)_{12}]^{5+}$ eluted next followed by the purple aqua ion and then later by the grayish purple $[Mo_7S_8(H_2O)_{18}]^{8+}$. The elution pattern is most consistent with the purple niobium aqua ion having a charge of $> +5$, probably +6 since it eluted closer to $[Mo_4S_4(H_2O)_{12}]^{5+}$ than to $[Mo_7S_8(H_2O)_{18}]^{8+}$.

Redox Titration. The average oxidation state of Nb in the purple aqua ion was determined by titration against cerium(IV) sulfate with ferroin as indicator.

Elemental Analyses. Carbon, hydrogen, and nitrogen analyses were determined by standard microanalytical procedures. Niobium was determined by either inductively coupled plasma atomic emission spectroscopy (ICP-AES) or inductively coupled plasma mass spectrometry (ICP-MS).

Cyclic Voltammetry. Cyclic voltammograms of the purple aqua ion were recorded on an edge-plane pyrolytic graphite electrode in the potential range −1.2 to +1.1 V using an Eco Chemie Autolab potentiostat. A coiled Pt-wire was used as counter electrode, and the reference electrode was a freshly prepared reversible hydrogen electrode. After each experiment, the reference electrode was checked against a saturated calomel electrode, and potentials were reported versus SCE.

EPR Spectroscopy. EPR spectrum was recorded on a Bruker EMX spectrometer with a 12 kW 10″ magnet equipped with a Bruker ER4102ST x-band cavity. A 90 mM (per Nb) solution of the purple aqua ion in 4 M HCl was cooled to 90 K by quenching a standard EPR quartz-tube (Wilmad) containing the sample into a glycerine-coated finger dewar flask, which was then placed directly in the cavity. The cavity was flushed continuously with inert gas to avoid water condensation and had a microwave frequency of 9.423 GHz.

DFT Calculations. The theoretical analysis of an electronic structure for the Nb_3 cluster was carried out by code ADF 2007.[15] The geometry optimization procedure was executed by the spin-restricted density-functional theory (DFT) method. The model Hamiltonians of the density functional are represented as a sum of the local density functional LDA (VWN[16]) and the gradient exchange functional GGA (Becke[17] and Perdew[18]). Basis sets consisted of Slater relativistic functions (TZP) without frozen cores. The Zero Order Regular Approximation (ZORA) was used to account for relativistic scalar effects.[19] The binding energies of the Nb_3 cluster complexes were defined by the Bickelhaupt and Baerends method.[20] Values of charges on atoms were obtained by use of the Hirshfeld method.[21] The electron density was analyzed with topological

(12) *SMART and SAINT, Area Detector Control and Integration Software*,Version 5.054; Bruker Analytical X-Ray Instruments Inc.: Madison, WI, 1998.

(13) Sheldrick, G. M. *SADABS, Program for Empirical Correction of Area Detector Data*, Version 2.03; University of Göttingen: Göttingen, Germany, 2001.

(14) Sheldrick, G. M. *SHELXTL, Structure Determination Programs*, Version 6.12; Bruker Analytical X-Ray Instruments Inc.: Madison, WI, 2001.

(15) *Amsterdam Density Functional (ADF) program*, Release 2007.02; Vrije Universteit: Amsterdam, The Netherlands, 2007.

(16) Vosko, S. H.; Wilk, L.; Nusair, M. *Can. J. Phys.* **1980**, *58*, 1200–1211.

(17) Becke, A. D. *Phys. Rev. A.* **1988**, *38*, 3098–3100.

(18) Perdew, J. P. *Phys. Rev.B.* **1986**, *33*(N12), 8822–8824.

(19) van Lenthe, E.; Ehlers, A. E.; Baerends, E. J. *J. Chem. Phys.* **1999**, *110*, 8943–8953.

(20) Bickelhaupt, F. M., Baerends, E. J. In *Reviews in computational chemistry*; Lipkowitz, K. B., Boyd, D. B., Eds.; Wiley-VCH: New York, 2000; Vol. *15*, pp 1−86.

(21) Hirshfeld, F. L. *Theor.Chim.Acta* **1977**, *44*, 129–138.

methods of quantum chemistry based on Bader's theory of Atoms in Molecules − QTAIM,[22] where analysis of critical points was carried out using the Xaim software developed by Jose Carlos Ortiz and Carles Bo, Universitat Rovira i Virgili, Tarragona, Spain.

Results and Discussion

Synthesis and Solution Properties. The isolation of the purple niobium aqua ion corroborates our view that there is a rich chemistry for niobium in aqueous solutions although only four niobium aqua ions have so far been reported.[7−10] The incorporation of acetonitrile in the cluster core is unexpected and unprecedented for a cluster aqua ion of any type.

Guy and Perron reported the synthesis of $NbCl_4 \cdot 3CH_3CN$ by the reduction of $NbCl_5$ in acetonitrile with Al and the subsequent use as an intermediate in the synthesis of other Nb(IV) compounds.[23] In these syntheses the weakly coordinated CH_3CN were readily replaced by other ligands. The X-ray crystal structure revealed that $NbCl_4 \cdot 3CH_3CN$ contain *cis* octahedral $[NbCl_4(CH_3CN)_2]$ and a solvent CH_3CN molecule. Hence, we were indeed surprised when CH_3CN ended up as a μ_3-ligand in a triangular $Nb(IV)_3$ cluster (see below) upon acid hydrolysis of Al-reduced $NbCl_5$ in acetonitrile.

During cation-exchange chromatography in aqueous HCl solutions, a purple species (most likely chloro species of the purple niobium aqua ion) eluted in 1 M HCl followed by the elution of the purple niobium aqua ion in 2 M HCl. Similar behavior has been observed for $[Mo_3O_4(H_2O)_9]^{4+}$ and was attributed to the formation of $[Mo_3O_4(H_2O)_{9-n}Cl_n]^{(4-n)+}$ species.[24] A dark reddish purple band remained bound from which several purple species continued eluting upon further washing with 3 or 4 M HCl until most of the color disappeared. When cation-exchange chromatography was carried out with non-coordinating HPTS, a purple fraction eluted in 2 M HPTS while a dark reddish purple band remained bound which could not be eluted even with 4 M HPTS. However, when 3−4 M HCl was used purple fractions began eluting from the dark reddish purple band. All the purple species described here have similar UV−visible spectra. The behavior of the purple aqua ion on a Dowex 50W-X2 cation-exchange column suggests a high extent of possibly dimerization or oligomerization of the purple aqua ion. This points toward high acidity of the coordinated water ligands, which could be expected for the electron deficient d^1 Nb(IV) centers. Available empty π-acceptor orbitals on each Nb(IV) could then readily stabilize a deprotonated water ligand as is the case for electron-deficient high-oxidation-state metal ions. The formation of dimers or oligomers of the cluster aqua ion through hydroxide bridges can be anticipated, hence resulting in the highlighted chromatographic properties.

The UV−visible spectrum of the purple aqua ion is very sensitive to the concentration of HCl, and in 2 M HCl (see Figure 1) a small peak at 365 nm ($\varepsilon \sim 511\ M^{-1}\ cm^{-1}$ per Nb)

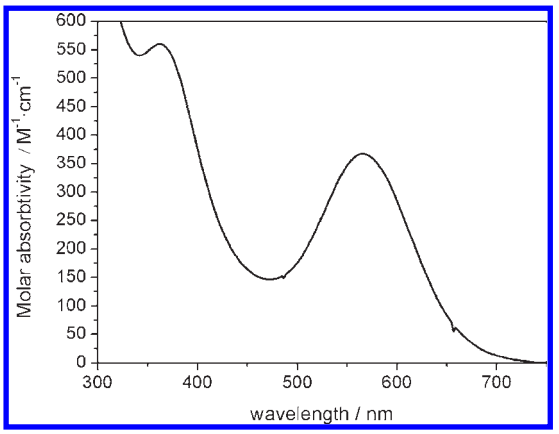

Figure 1. Electronic spectrum of $[Nb_3(\mu\text{-}\eta^2\text{:}\eta^2\text{-}NCCH_3)O_3(H_2O)_9]^{6+}$ in 2 M HCl.

and a broad peak at 565 nm ($\varepsilon \sim 335\ M^{-1}\ cm^{-1}$ per Nb) are observed. Both $[Cl^-]$ and $[H^+]$ appear to influence the UV−visible spectrum of the purple niobium aqua ion. Upon varying $[Cl^-]$ from 0.6 to 4.9 M, the peak at 565 nm appeared essentially unchanged while the shoulder at about 360 nm developed into a clear peak resulting in about a 20% increase in absorbance. Surprisingly, varying $[H^+]$ has a more dramatic effect; the shoulder at 360 nm developed into a large peak at 375 nm with $a > 100\%$ increase in absorbance upon increasing $[H^+]$ from 0.6 to 4.9 M. At the same time, a significant red shift by about 25 nm was observed for the 565 nm peak. Clearly both $[Cl^-]$ and $[H^+]$ have an influence on the UV−visible spectrum. The effect of Cl^- most likely stems from ligand exchange between H_2O and Cl^-. The change in spectrum upon varying $[H^+]$ suggests involvement of protonation-deprotonation and could well be due to the formation of hydroxo species. However, absorbance changes of this size are usually not observed for such a process. The protonation of the N atom of the μ_3-CH_3CN could be a plausible cause but DFT calculations do not favor protonation of the CH_3CN over the deprotonated form.

The purple aqua ion is EPR-active ($g = 1.98$) but no hyperfine interaction with the ^{93}Nb nuclear spin ($I = 9/2$) was observed. Other Nb(IV) complexes which do not show hyperfine interactions with niobium in their EPR spectra have been previously reported.[10,25]

X-ray Crystal Structure of $((CH_3)_3NH)_3[Nb_3(\mu\text{-}\eta^2\text{:}\eta^2\text{-}NCCH_3)O_3(NCS)_9]\cdot 2.5H_2O$ (1). The technique of X-ray structure analysis is crucial in identifying the structure of metal-cluster compounds. Whereas previously aqua ions of metal clusters have been notoriously difficult to crystallize, in the last 2 decades approaches for crystallization of such aqua ions particularly for molybdenum and tungsten have been achieved. One approach is by using cation-exchange chromatography to achieve concentrated solutions of the aqua ion in the non-coordinating acid, HPTS (para-toluenesulfonic acid).[26] The second is a supramolecular approach using the macrocyclic

(22) Bader, R. F. *Atoms in Molecules: A Quantum Theory*; Clarendon: New York, 1990.
(23) Gut, R.; Perron, W. *J. Less-Common Metals* **1972**, *26*, 369–379.
(24) Kathirgamanathan, P.; Soares, A. B.; Richens, D. T.; Sykes, A. G. *Inorg. Chem.* **1985**, *24*, 2950–2954.
(25) Lucas, D.; Mugnier, Y.; Antiñolo, A.; Otero, A.; Garcia-Yuste, S.; Fajardo, M. *J. Organomet. Chem.* **1995**, *490*, 7–10.
(26) See for example: Shibahara, T.; Takeuchi, A.; Ohtsuji, A.; Kohda, K.; Kuroya, H. *Inorg. Chim. Acta* **1987**, *127*, L45–46. Akashi, H.; Shibahara, T.; Kuroya, H. *Polyhedron* **1990**, *9*, 1671–1676. Richens, D. T.; Helm, L.; Pittet, P. A.; Merbach, A. E.; Nicolo, F.; Chapuis, G. *Inorg. Chem.* **1989**, *28*, 1394–1402.

cavitands cucurbit[n]uril, which requires formation of favorable hydrogen-bonding network to give the supramolecular adducts of the cluster aqua ion and cucurbituril.[27] Although these methods have been used successfully for, for example, $[M_3Y_4(H_2O)_9]^{4+}$ and $[M_4Y_4(H_2O)_{12}]^{5+}$ (M = Mo or W, Y = O or S), they failed in the case of our purple aqua ion. Because of the higher charge and problems with hydrolysis and the associated oligomerization, concentrated solutions in HPTS could not be obtained. The supramolecular approach yielded no suitable crystals either. Hence, the earliest widely accepted approach of obtaining crystals of complexes by the substitution of the aqua ligands by other ligands such as thiocyanate[28] has been employed for X-ray structure analysis here. The assumption that the core structure of the cluster aqua ion remained intact in the ligand substitution reaction has been proven to be valid for the molybdenum and tungsten cluster aqua ions mentioned above,[26,28] and there is no reason to think otherwise for our purple niobium aqua ion.

The X-ray structural analysis of **1** prepared from the reaction of the purple aqua ion with thiocyanate revealed an unprecedented trinuclear core structure, $Nb_3(\mu\text{-}\eta^2\text{:}\eta^2\text{-}NCCH_3)O_3^{6+}$, in the $[Nb_3(\mu\text{-}\eta^2\text{:}\eta^2\text{-}NCCH_3)O_3(NCS)_9]^{3-}$ anion (Figure 2). Noteworthy is the unusual coordination mode of the acetonitrile, whereby the lone pair on the nitrogen atom do not participate in the coordination, very much in the same fashion as that reported in the ruthenium nitrile complex, $(Cp^*Ru)_3(\mu_3\text{-}\eta^2\text{:}\eta^2(\perp)\text{-RCN})(\mu_3\text{-H})(\mu\text{-H})_2$.[5] The μ_3-nitrile ligand of $(Cp^*Ru)_3(\mu_3\text{-}\eta^2\text{:}\eta^2(\perp)\text{-RCN})(\mu_3\text{-H})(\mu\text{-H})_2$ readily undergoes reversible protonation to afford the μ_3-iminoacyl complex. Since hydrogen atoms in **1** cannot be located, the alternative species, $[Nb_3(\mu\text{-}\eta^2\text{:}\eta^2\text{-HNCCH}_3)O_3(NCS)_9]^{3-}$, whereby the bridging CH_3CN ligand is protonated cannot be ruled out. However, on the basis of results from DFT calculations, oxidation state determination, and EPR studies (see below), the unprotonated form is favored. In contrast to the electron-rich $Ru(II)_3$ (d^{18}) cyclopentadienyl complex, our electron-deficient $Nb(IV)_3$ (d^3) cluster is less basic, hence less likely to protonate. What is surprising is that although the triniobium complex is relatively electron poor, the nitrile ligand acts as a 4e donor rather than as a 6e donor found in the triiron carbonyl complex, $Fe_3(CO)_9(\mu_3\text{-}\eta^1\text{:}\eta^2\text{:}\eta^2\text{-RCN})$.[29] In the triiron complex, the nitrogen atom of the nitrile ligand is directed inside the Fe_3 core with additional κN coordination, whereas in the triruthenium complex and our triniobium complex the nitrile ligands are bound in the direction opposite to that found in the triiron complex with the lone pair on the nitrogen atom not participating in bonding. Hence, other factors such as steric effects probably play a role in determining the coordination mode of the nitrile.

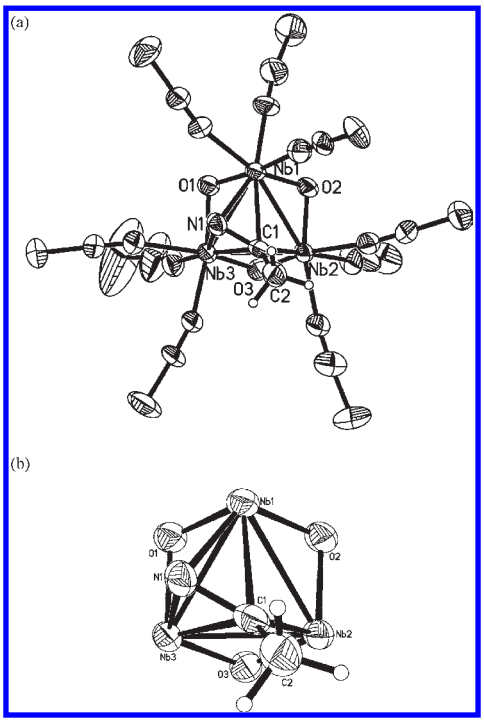

Figure 2. Perspective view of $[Nb_3(\mu\text{-}\eta^2\text{:}\eta^2\text{-}NCCH_3)O_3(NCS)_9]^{3-}$ anion. The thermal ellipsoids are drawn at 50% probability level. (b) An enlarged view of the $Nb_3(\mu\text{-}\eta^2\text{:}\eta^2\text{-}NCCH_3)O_3^{6+}$ core.

Selected bond distances and angles for the $[Nb_3(\mu\text{-}\eta^2\text{:}\eta^2\text{-}NCCH_3)O_3(NCS)_9]^{3-}$ anion are given in Table 2. The trinuclear cluster consists of a triangular $Nb_3(\mu_2\text{-}O_3)$ unit of the type previously seen in the $[Nb_3SO_3(NCS)_9]^{6-}$ anion. All three niobium interactions are bonding (2.8191(11), 2.8883(11), and 2.8184(12) Å), and are each bonded to three terminal thiocyanate ligands and two μ-oxo groups. The Nb1−Nb3 (2.8883(11)Å) bond distance is significantly longer than the Nb1−Nb2 and Nb2−Nb3 bond distances of 2.8191(11) and 2.8184(12) Å, respectively. However, the bond distances are well within those observed for triangular niobium cluster complexes previously reported, for example, 2.833(7) Å in $[Nb_3(\mu_3\text{-}O)_2(\mu\text{-}O_2CMe)_6(thf)_3]^+$,[30] 2.857(5)Å in $[Nb_3(\mu\text{-}Cl)_3(\mu\text{-}O)_3(\eta^5\text{-}C_5Me_5)_3]^+$,[31] 2.870(6) and 2.885(5)Å in $[Nb_3(\mu_3\text{-}O)_2(\mu\text{-}SO_4)_6(H_2O)_3]^{5-}$,[30,32] and 2.976(6)Å in $[Nb_3(\mu_3\text{-}Cl)(\mu_2\text{-}Cl)_3Cl_6(PEt_3)_3]^-$.[33] The determined charge of the complex indicates a d^3 electronic configuration for the Nb_3 core, hence giving Nb−Nb bond order of 1/2.

The remarkable feature of the structure, is the capping of the open face of the $Nb_3(\mu_2\text{-}O_3)$ cluster by an unusual $(\mu\text{-}\eta^2\text{:}\eta^2\text{-}NCCH_3)$ ligand, instead of a μ_3-S ligand. The C−N bond of the μ_3-CH_3CN is positioned on a plane through N1, C1, C2, and Nb2. This plane is nearly perpendicular to the plane through Nb1, Nb2, and Nb3,

(27) See for example: Fedin, V. P.; Virovets, a.V.; Sokolov, M. N.; Dybtsev, D. N.; Gersako, O. A.; Clegg, W. *Inorg. Chem.* **2000**, *39*, 2227–2230. Sokolov, M. N.; Virovets, A. V.; Dybtsev, D. N.; Gerasko, O. A.; Fedin, V. P.; Hernandez-Molina, R.; Clegg, W.; Sykes, A. G. *Angew. Chem., Int. Ed.* **2000**, *39*, 1659–1661. Fedin, V. P.; Virovets, A. V.; Dybtsev, D. N.; Gerasko, O. A.; Hegetschweiler, K.; Elsegood, M. R. J.; Clegg, W. *Inorg. Chim. Acta* **2000**, *304*, 301–304. Fedin, V. P.; Sokolov, M. N.; Dybtsev, D. N.; Virovets, A. V.; Clegg, W.; Fedin, V. P. *Russ. Chem. Bull., Int. Ed.* **2001**, *7*, 1144–1147.

(28) Murmann, R. K.; Shelton, M. E. *J. Am. Chem. Soc.* **1980**, *102*, 3984–3985. Shibahara, T.; Yamada, T.; Kuroya, H.; Hills, E. F.; Kathirgamanathan, P.; Sykes, A. G. *Inorg. Chim. Acta* **1986**, *113*, L10–21. Shibahara, T.; Kohda, K.; Ohtsuji, A.; Yasuda, K.; Kuroya, H. *J. Am. Chem. Soc.* **1986**, *108*, 2756–2758.

(29) Andrews, M. A.; Knobler, C. B.; Kaesz, H. D. *J. Am. Chem. Soc.* **1979**, *101*, 7260–7264.

(30) Cotton, F. A.; Diebold, M. P.; Roth, W. J. *Inorg. Chem.* **1988**, *27*, 2347–2352.

(31) Bottomley, F.; Karslioglu, S. *J. Chem. Soc., Chem. Commun.* **1991**, 222–223.

(32) Bino, A. *Inorg. Chem.* **1982**, *21*, 1917–1920.

(33) Cotton, F. A.; Diebold, M. P.; Feng, X.; Roth, W. J. *Inorg. Chem.* **1988**, *27*, 3413–3421.

Table 2. Selected Bond Distances (Å) and Bond Angles (deg) in $((CH_3)_3NH)_3[Nb_3(\mu\text{-}\eta^2\text{:}\eta^2\text{-}NCCH_3)O_3(NCS)_9]\cdot 2.5H_2O$ (**1**)

Bond Distances					
		Nb−Nb			
Nb1−Nb2	2.8191(11)	Nb1−Nb3	2.8883(11)	Nb2−Nb3	2.8184(12)
		Nb-μO			
Nb1−O1	2.031(7)	Nb2−O2	1.936(6)	Nb3−O1	2.046(6)
Nb1−O2	1.943(6)	Nb2−O3	1.922(7)	Nb3−O3	1.942(6)
		Nb-CH$_3$CN			
Nb1−N1	2.106(8)	Nb3−N1	2.123(8)		
Nb1−C1	2.391(9)	Nb3−C1	2.413(10)	Nb2−C1	2.138(10)
		Nb-NCS			
Nb1−N1A	2.160(8)	*trans* N1			
Nb1−N2A	2.131(9)	*trans* O1			
Nb1−N3A	2.209(8)	*trans* O2			
Nb2−N1B	2.167(10)	*trans* O2			
Nb2−N2B	2.195(9)	*trans* O3			
Nb2−N3B	2.204(9)	*trans* C1			
Nb3−N1C	2.206(8)	*trans* O3			
Nb3−N2C	2.123(9)	*trans* O1			
Nb3−N3C	2.158(11)	*trans* N1			
C1−N1	1.372(11)				
C1−C2	1.500(14)				

Bond Angles			
Nb1−N1−Nb3	86.2(3)	Nb1−O1−Nb3	90.2(3)
Nb1−C1−Nb2	76.8(3)	Nb1−O2−Nb2	93.2(3)
Nb1−C1−Nb3	73.9(3)	Nb2−O3−Nb3	93.7(3)
Nb2−C1−Nb3	76.3(3)		
Nb2−C1−C2	119.1(7)		
Nb2−C1−N1	125.9(7)		
N1−C1−C2	115.0(9)		

the angle between the two planes being 88.1(2)°. Like in $(Cp^*Ru)_3(\mu_3\text{-}\eta^2\text{:}\eta^2(\perp)\text{-}RCN)(\mu_3\text{-}H)(\mu\text{-}H)_2$,[5] where the C−N bond is disposed on the crystallographic mirror plane, the (N1, C1, C2, Nb2)-plane bisects the Nb_3 triangle with the nitrogen atom oriented to the outside of the Nb_3 core, which is opposite to that observed in $Fe_3(CO)_9(\mu_3\text{-}\eta^1\text{:}\eta^2\text{:}\eta^2\text{-}RCN)$,[29] $Nb_3Cl_8(t\text{-}BuNC)_5$,[34] and $[Fe_3(CO)_9(\mu_3\text{-}\eta^2\text{-}CNBu^t)]$.[35] The CH_3CN is μ-bonded (π-bonded) to both Nb1 and Nb3 via the two orthogonal nitrile π-bonds with Nb1−N1 and Nb3−N1 distances of 2.106(8) and 2.123(8) Å, respectively, and Nb1−C1 and Nb3−C1 distances of 2.391(9) and 2.413(9) Å, respectively. At the same time it is σ-bonded to Nb2 at a Nb2−C1 at 2.138(10) Å. The bond lengths between the niobium atoms and the nitrile carbon indicate bonding interactions between all the niobium atoms and the nitrile carbon. The angles Nb2−C1−C2, Nb2−C1−N1, and C2−C1−N1 at 119.1(7), 125.9(7), and 115.0(9), respectively, are close to the ideal value for sp^2 -hybridized atoms. The ligand carbon−nitrogen distance of 1.374(11) Å is significantly longer than that of a C−N triple bond (1.16 Å) and lies in between that of a C−N double bond (1.28 Å) and that of a C−N single bond (1.47 Å).[36] This implies that there is strong back-donation to the nitrile ligand despite the low electron count for the Nb_3 framework which is counteracted by the presence of the electron-rich thiocyanate and oxo ligands. This bond distance is close to that of the C−N distance of 1.358(6) Å for the electron-rich triruthenium complex, which contains electron-releasing Cp groups.

DFT Calculations. Since the crystal structure cannot unambiguously pin down the species, $[Nb_3(\mu\text{-}\eta^2\text{:}\eta^2\text{-}NCCH_3)O_3(NCS)_9]^{3-}$ (**I**) in favor of $[Nb_3(\mu\text{-}\eta^2\text{:}\eta^2\text{-}HNCCH_3)O_3(NCS)_9]^{3-}$ (**II**), whereby the bridging CH_3CN ligand is protonated, a theoretical analysis of the electronic structure of both was carried out. The optimized values of the structural parameters of both (**I**) and (**II**) are within satisfactory agreement with the experimental data (see Supporting Information). The binding energies of −281.4 eV for (**I**) and −286.3 eV for (**II**) suggest that both (**I**) and (**II**) can exist. However, energy level diagrams of molecular orbitals (MOs) given in Figure 3, clearly shows that (**I**) is paramagnetic whereas the complex (**II**) is diamagnetic as the 217A MO is half-filled for (**I**) and is completely filled for (**II**). Hence, $[Nb_3(\mu\text{-}\eta^2\text{:}\eta^2\text{-}NCCH_3)O_3(NCS)_9]^{3-}$ with the unprotonated

(34) Cotton, F. A.; Roth, W. J. *J. Am. Chem. Soc.* **1983**, *105*, 3734–3735.
(35) Bruce, M. I.; Hambley, T. W.; Nicholson, B. K. *J. Chem. Soc., Chem. Commun.* **1982**, 353–355.
(36) *International Tables for Crystallography*; Kluwer Academic Publishers: Dordrecht/Boston/London, 1999; Vol. *C*, pp 794−795.

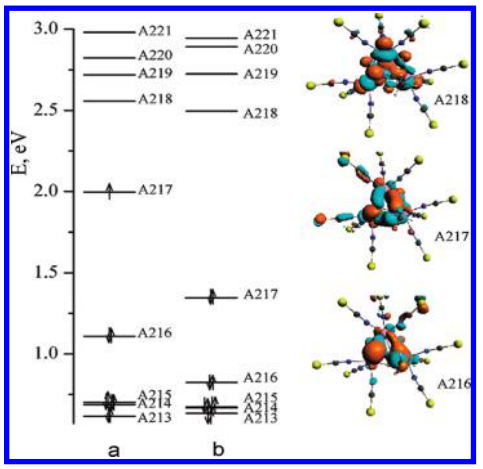

Figure 3. Diagram of MO levels (left): (a) $[Nb_3(\mu\text{-}\eta^2\text{:}\eta^2\text{-}NCCH_3)O_3(NCS)_9]^{3-}$ (**I**); (b) $[Nb_3(\mu\text{-}\eta^2\text{:}\eta^2\text{-}HNCCH_3)O_3(NCS)_9]^{3-}$ (**II**). Images of the active molecular orbitals (right).

μ_3-CH_3CN is most consistent with the observed EPR-activity.

The highest occupied molecular orbital (HOMO, 217A MO) consists of mainly contribution from 4d orbitals of the three Nb atoms (~41%), 2p orbitals of O2 and O3 atoms (~7%), including N1 2p orbitals (~7%) and C1 2p orbitals (~15%) of CH_3CN in (**I**). The atom N1 of CH_3CN has bonding interaction with Nb1 and Nb3. The atom C1 of CH_3CN has bonding interaction with Nb1, Nb3, and Nb2. Thus, the unpaired electron is located not only on Nb atoms of the Nb_3 cluster but also delocalized onto the CH_3CN ligand, suggesting that CH_3CN is excited. This result may explain the deformed structure of CH_3CN in the crystal structure. The energy gap between HOMO−LUMO is 0.56 eV.

The HOMO of (**I**) shows that atom N1 is characterized by bonding with three atoms: C1, Nb1, and Nb3 whereas atom C1 is characterized by bonding interaction with five atoms: C2, N1, Nb1, Nb3, and Nb2. This result agrees well with data obtained by the topological method of quantum chemistry − QTAIM (see Supporting Information).

$[Nb_3(\mu\text{-}\eta^2\text{:}\eta^2\text{-}NCCH_3)O_3(H_2O)_9]^{6+}$ Aqua Ion. Aliquots of the purple aqua ion titrated with standard $Ce(SO_4)_2$ gave an average oxidation number of +3.85 ± 0.25 from four determinations which does not allow an unambiguous assignment of oxidation state since this value lies midway between +3.67 for an assignment of $Nb(IV)_2Nb(III)$ and +4 for $Nb(IV)_3$. However, the X-ray structure analysis, DFT calculations, and EPR results best agree with the existence of the $[Nb_3(\mu\text{-}\eta^2\text{:}\eta^2\text{-}NCCH_3)O_3(H_2O)_9]^{6+}$ aqua ion in solution, which upon reaction with thiocyanate gives $[Nb_3(\mu\text{-}\eta^2\text{:}\eta^2\text{-}NCCH_3)O_3(NCS)_9]^{3-}$. This is also consistent with the charge determination experiment where the purple niobium aqua ion has an estimated charge of +6.

Cyclic Voltammetry of $[Nb_3(\mu\text{-}\eta^2\text{:}\eta^2\text{-}NCCH_3)O_3(H_2O)_9]^{6+}$. The cyclic voltammogram of 9 mM (per Nb) $[Nb_3(\mu\text{-}\eta^2\text{:}\eta^2\text{-}NCCH_3)O_3(H_2O)_9]^{6+}$ in 4 M HCl on edge-plane pyrolytic graphite electrode at a scan rate of 50 mV s^{-1} in the potential range −1.2 V to +1.1 V (Figure 4, solid line) exhibits three anodic peaks at −0.12, +0.53, and +0.85 V (labeled peaks 1, 2, and 3) and a large cathodic peak at −0.91 V (peak 5) with a slight shoulder at about −0.8 V (peak 4). Further investigation in three different potential windows (Figure 4) revealed that the cathodic

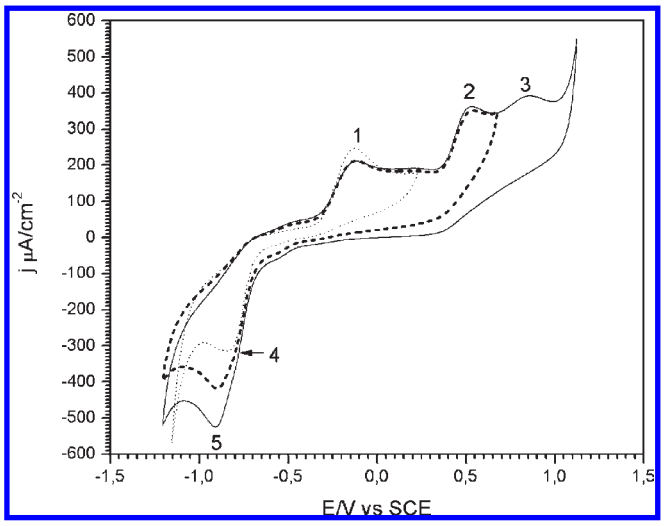

Figure 4. Cyclic voltammogram of 9 mM $[Nb_3(\mu\text{-}\eta^2\text{:}\eta^2\text{-}NCCH_3)O_3(H_2O)_9]^{6+}$ in 4 M HCl on edge-plane pyrolytic graphite electrode upon scanning at 50 mV s^{-1} in three different potential windows (solid line from −1.2 to +1.1 V, dashed line from −1.2 to +0.7 V, and dotted line from −1.15 to +0.2 V). The peaks are numbered from 1 to 5 and are referred to in the main text.

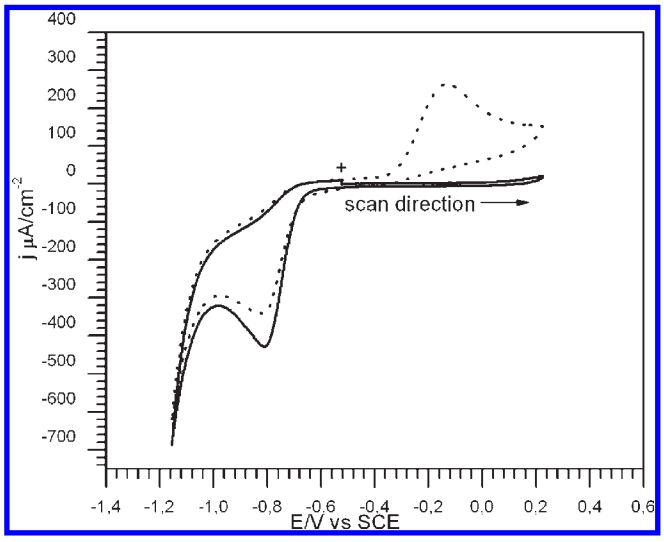

Figure 5. Cyclic voltammogram of 9 mM $[Nb3(\mu\text{-}\eta^2\text{:}\eta^2\text{-}NCCH_3)O_3(H_2O)_9]^{6+}$ in 4 M HCl on edge-plane pyrolytic graphite electrode upon scanning at 50 mV s^{-1} from −1.15 to +0.2 V (solid line is first scan, dotted line is second scan).

peak is related to all three anodic peaks since the cathodic peak current increases concurrent with scanning further toward positive potentials.

In the narrow potential window −1.2 V to +0.3 V, the cyclic voltammogram shows only a cathodic peak in the first scan whereas subsequent scans exhibit both an anodic (peak 1) as well as a cathodic peak (peak 4), see Figure 5. Peaks 1 and 4 constitute a redox couple (redox couple I) given the peak symmetry and similar charge for both peaks, with the oxidized form of the redox couple corresponding to the starting complex. The peak widths are most consistent with 1e transfer. The formal reduction potential is estimated to be −0.48 V, and the rather large peak−peak separation of about 0.7 V completely rules out a reversible process but is suggestive of a quasi-reversible process since the charges under the anodic

and cathodic peaks are similar. The fact that the anodic and cathodic peaks are far from the equilibrium potential at −0.48 V suggests that large overpotentials are required to overcome the energy barriers for reduction and oxidation.

Cyclic voltammetry in the slightly wider potential window of −1.2 to 0.7 V (Figure 4, dashed line) shows two anodic peaks at −0.12 and 0.53 V and a cathodic peak at −0.89 V with a slight shoulder at −0.79 V. An analysis of total current transferred revealed that the total charge for peaks 1 and 2 accords well with the total charge under the unresolved peaks 4 and 5. The good correspondence between the total area of the anodic and cathodic peaks points toward an equal number of electron being transferred in the oxidation and reduction reactions, which suggests that peaks 2 and 5 constitute yet another redox pair (redox couple II). The peak−peak separation of 1.42 V is even wider than for couple I. Couple II appears to be electrochemically irreversible, but once again since the charges under the anodic and cathodic peaks agree it is more appropriately described as a quasi-reversible system.

Cyclic voltammetry in the potential range −1.2 V to +1.1 V (Figure 4, solid line) shows very characteristic features with anodic peaks at −0.12 V, +0.53 V, and +0.85 V and a cathodic peak at −0.90 V with a shoulder at −0.79 V. The total amount of charge associated with anodic peaks 1, 2, and 3 corresponds well to the total charge of cathodic peaks 4 and 5. The good correspondence between the areas of the anodic and cathodic peaks points toward all three anodic peaks being tied to the two cathodic peaks. Hence peaks 1 and 4 form one redox couple (eq 1), while peaks 2 and 5 (eq 2) and peaks 3 and 5 (eq 3) constitute two further redox processes, redox couples II and III, respectively. The cathodic peaks of II and III overlap too much to enable a distinction between them in the cyclic voltammogram.

The peaks in the cyclic voltammogram of $[Nb_3(\mu\text{-}\eta^2{:}\eta^2\text{-}NCCH_3)O_3(H_2O)_9]^{6+}$ (Figure 4, solid line) can thus be simplistically assigned to the electron transfer reactions as below:

$$Nb^{IV}{}_3 - e^- = Nb^{IV}{}_2Nb^V \quad (1)$$

$$Nb^{IV}{}_2Nb^V - e^- = Nb^{IV}Nb^V{}_2 \quad (2)$$

$$Nb^{IV}Nb^V{}_2 - e^- = Nb^V{}_3 \quad (3)$$

However, since DFT calculations show that the unpaired electron is delocalized among the three Nb atoms as well as CH_3CN, an involvement of the CH_3CN ligand is most likely to be the case. The fact that large overpotentials are required to overcome the energy barriers for reduction and oxidation (viz., large peak−peak separations) for all three redox couples is probably due to a disruption of the bonding pattern between the Nb_3O_3 moiety and the μ_3-CH_3CN ligand. It can be anticipated that the already electron deficient $Nb_3(\mu\text{-}\eta^2{:}\eta^2\text{-}NCCH_3)O_3{}^{6+}$ core would be unstable upon losing electrons resulting in structural changes, most likely involving the opening and closing of the cluster at the μ_3-CH_3CN position.

Conclusion

In conclusion, we have prepared a triniobium aqua ion containing a perpendicularly coordinated μ_3-nitrile ligand which acts as 4e donor. This mode of coordination has so far only been reported for $(Cp^*Ru)_3(\mu_3\text{-}\eta^2{:}\eta^2(\perp)\text{-}RCN)(\mu_3\text{-}H)(\mu\text{-}H)_2$ where the highly electron-rich ruthenium centers coupled with the electron-releasing Cp* groups has been thought to be responsible for enabling such unusual coordination of a nitrile ligand. Here, we have a formally electron deficient triniobium center. Substantial electron delocalization from μ_2-O's as well as either H_2O or NCS^- ligands could be expected to contribute toward stabilization of unusual 4e-nitrile coordination. Last but not least, the $[Nb_3(\mu\text{-}\eta^2{:}\eta^2\text{-}NCCH_3)O_3(H_2O)_9]^{6+}$ aqua ion is the first organometallic cluster aqua ion to be reported and is the only example of an organometallic species with several peripheral ligands around each metal which are all completely water ligands.

Acknowledgment. The authors thank Dr. Zhang Jingdong for help in cyclic voltammetric experiments and Prof. Jens Ulstrup for helpful discussions on electrochemistry, Dr. Søren Birk Rasmussen for help in recording the EPR spectrum, Dr. Jens E.T. Andersen for help with niobium analysis, and the Technical University of Denmark for an H.C. Ørsted Postdoctoral Fellowship to A.L.G.

Supporting Information Available: Dependence of UV−visible spectrum of $[Nb_3(\mu\text{-}\eta^2{:}\eta^2\text{-}NCCH_3)O_3(H_2O)_9]^{6+}$ aqua ion on $[H^+]$ and $[Cl^-]$. EPR spectrum of $[Nb_3(\mu\text{-}\eta^2{:}\eta^2\text{-}NCCH_3)O_3(H_2O)_9]^{6+}$ aqua ion. Computational details for DFT analysis. This material is available free of charge via the Internet at http://pubs.acs.org.